



Large-scale climatic and geophysical controls on the leaf economics spectrum

Gregory P. Asner^{a,1}, David E. Knapp^a, Christopher B. Anderson^a, Roberta E. Martin^a, and Nicholas Vaughn^a

^aDepartment of Global Ecology, Carnegie Institution for Science, Stanford, CA 94305

Contributed by Gregory P. Asner, May 27, 2016 (sent for review March 29, 2016; reviewed by Alex Held and John W. Terborgh)

Leaf economics spectrum (LES) theory suggests a universal trade-off between resource acquisition and storage strategies in plants, expressed in relationships between foliar nitrogen (N) and phosphorus (P), leaf mass per area (LMA), and photosynthesis. However, how environmental conditions mediate LES trait interrelationships, particularly at large biospheric scales, remains unknown because of a lack of spatially explicit data, which ultimately limits our understanding of ecosystem processes, such as primary productivity and biogeochemical cycles. We used airborne imaging spectroscopy and geospatial modeling to generate, to our knowledge, the first biospheric maps of LES traits, here centered on 76 million ha of Andean and Amazonian forest, to assess climatic and geophysical determinants of LES traits and their interrelationships. Elevation and substrate were codominant drivers of leaf trait distributions. Multiple additional climatic and geophysical factors were secondary determinants of plant traits. Anticorrelations between N and LMA followed general LES theory, but topo-edaphic conditions strongly mediated and, at times, eliminated this classic relationship. We found no evidence for simple P-LMA or N-P trade-offs in forest canopies; rather, we mapped a continuum of N-P-LMA interactions that are sensitive to elevation and temperature. Our results reveal nested climatic and geophysical filtering of LES traits and their interrelationships, with important implications for predictions of forest productivity and acclimation to rapid climate change.

Amazon basin | functional biogeography | leaf traits | plant traits | tropical forests

In trait-based ecology, a “leaf economics spectrum” (LES) expresses an important trade-off in resource acquisition and storage strategies in plants (1). At one end of the spectrum, a strategy promoting rapid carbon gain via photosynthesis is underpinned by high foliar concentrations of nutrients, such as nitrogen (N) and phosphorus (P). This strategy is common in higher-fertility ecosystems, and it is linked to rapid foliar turnover via abscission and herbivory that maintains relatively fast rates of nutrient cycling (2, 3). At the other end of the spectrum, a plant strategy of lower foliar nutrient concentrations and slower plant growth in relatively low-fertility ecosystems invests proportionally more into leaf construction, expressed as higher leaf mass per unit area (LMA) (4), supporting longer-lived foliage and slower decomposition rates (5). Central to the LES theory, plants are thought to fall along simple axes indicating this trade-off, with important implications for global dynamic vegetation and climate models (6).

For LES rules to work in biospheric models, relationships between the key plant traits must be consistent (or at least known) across prevailing environmental conditions, such as climate and substrate fertility (7, 8). However, the geography of—and thus the geophysical controls over—LES traits remain poorly understood (9). To date, field sampling has established mostly cross-biome relationships between LES traits and climate (10). Global leaf trait databases obtained from plot-based measurements have been insufficient to develop spatially explicit knowledge of the environmental conditions under which LES trait interrelationships change. Establishing a LES geography would advance our knowledge of environmental controls on ecosystem functioning,

and support the next generation of biospheric models that incorporate plant traits.

Perhaps nowhere is our understanding of the LES weaker than in the tropical forest biome. The general inaccessibility of tropical forests, combined with an enormous pool of species, limits large-scale interpretation of LES data taken from field studies. Data scarcity also shortchanges the global databases with relatively limited tropical representation (1, 11), which is problematic given that environmental conditions vary widely throughout the biome (12). Fortunately, new maps of potential environmental filters of LES traits are becoming available. Such maps reveal numerous combinations of topographic, hydrologic, geologic, and climatic conditions, some of which display abrupt changes (e.g., where different geologic surfaces meet), whereas others undergo spatially continuous change (e.g., air temperature with elevation). Pairing climatic and geophysical maps with spatially explicit data on LES traits could reveal the strength and direction of key controls, thereby providing insight to the functional assembly of the biosphere.

Airborne imaging spectroscopy is emerging as an approach for mapping LES traits at scales ranging from individual plants to large landscapes (13, 14). Imaging spectrometers measure the solar radiation reflected from a surface in narrow, contiguous, and overlapping spectral channels covering a broad wavelength range, such as 350–2,500 nm (15). High-fidelity imaging spectrometers, which are currently rare, provide spectral reflectance data that can yield estimates of multiple canopy foliar traits with demonstrable precision and accuracy (16). Recent progress in fusing imaging spectrometer data with coaligned light detection and ranging (LiDAR) data on plant canopy structure yields estimates of trait suites that include N, P, and LMA, at spatial

Significance

Ecology seeks general principles describing how the biota respond to multiple environmental factors, partly to build a more prognostic science in the face of global climate change. One such principle to emerge is the “leaf economics spectrum” (LES), which relates ecologically important plant nutrients to leaf construction and growth along simple relational axes. However, interrelationships between LES traits have not been tested at large geographic scales. Using airborne imaging spectroscopy and geospatial modeling, we discovered strong climatic and geophysical controls on LES traits and their interrelationships throughout Andean and western Amazonian forest canopies. This finding highlights the need for biogeographically explicit treatment of plant traits, afforded by imaging spectroscopy, in the next generation of biospheric models.

Author contributions: G.P.A. designed research; G.P.A., D.E.K., C.B.A., R.E.M., and N.V. performed research; D.E.K., R.E.M., and N.V. contributed new reagents/analytic tools; G.P.A., D.E.K., C.B.A., R.E.M., and N.V. analyzed data; and G.P.A. and R.E.M. wrote the paper.

Reviewers: A.H., Commonwealth Scientific and Industrial Research Organization, Office of Space Science and Applications; and J.W.T., Duke University.

The authors declare no conflict of interest.

¹To whom correspondence should be addressed. Email: gpa@carnegiescience.edu.

This article contains supporting information online at www.pnas.org/lookup/suppl/doi:10.1073/pnas.1604863113/-DCSupplemental.

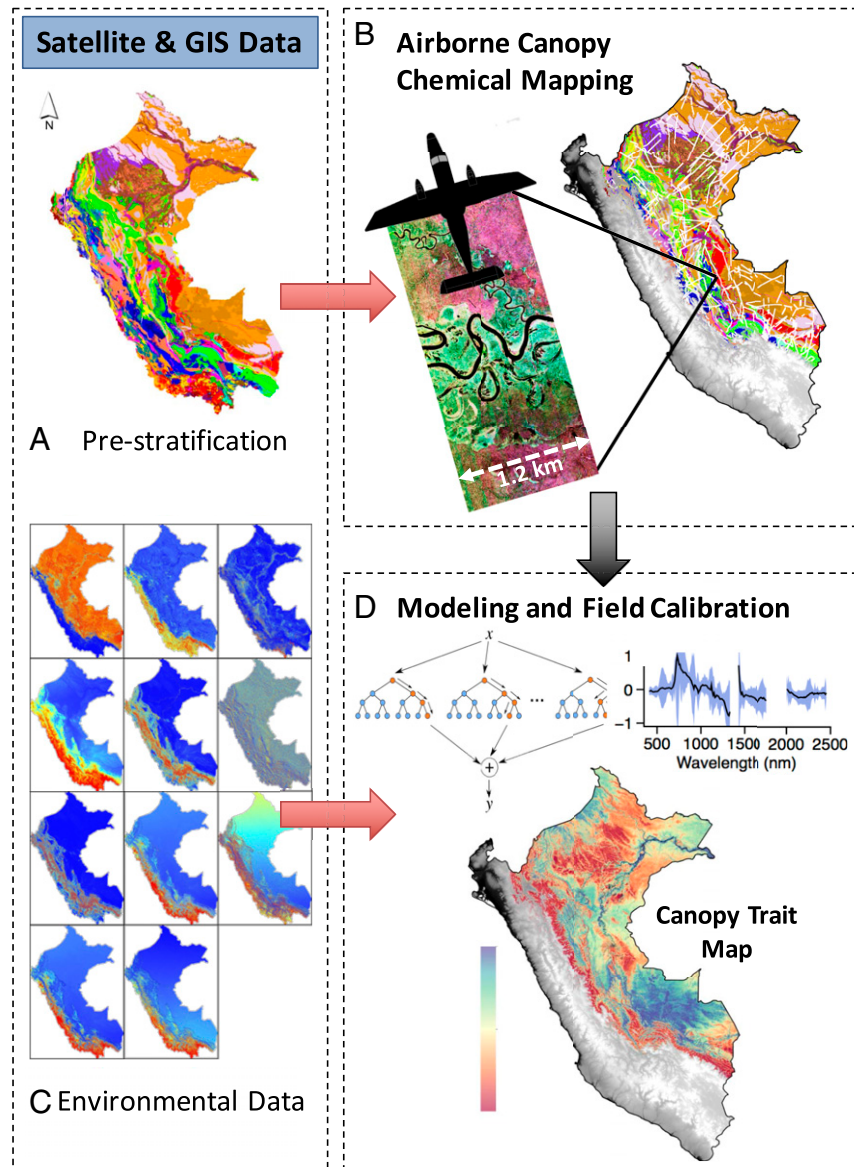


Fig. 1. Overview of the methodology used to map forest canopy traits throughout the country of Peru: (A) A prestratification step combined geological, soil, community floristic composition, elevation, and forest cover maps to forecast the potential range of environmental conditions to be encountered during airborne surveys. (B) The country was gridded into 100×100 -km sampling cells, and the CAO was used to sample each grid cell. CAO flightlines were 1.2-km wide with a ground sampling distance of 2.0 m. (C) A diverse array of satellite data were compiled and processed to provide continuous geographic information on geologic, topographic, and climate variables at 1-ha grid resolution. (D) The geospatial maps and CAO data were integrated using a geostatistical modeling approach based on Machine Learning, and combined with calibrations of CAO spectral data to field-estimated canopy trait determinations, to map canopy foliar N, P, and LMA at 1-ha resolution. The approach removes any nonforest canopy pixels from the CAO data, thereby providing model-based relationships between biogeophysical factors and canopy traits (Figs. S1–S4).

resolutions and geographic scales unachievable via field and laboratory approaches (17). However, the technology is limited to just a few aircraft, and thus has not been applied at very large scales.

We present, to our knowledge, the first maps of forest canopy LES traits over a large portion of the biosphere, here focused on western Amazonian and Andean forests. Our approach is based on airborne laser-guided imaging spectroscopy to derive wide-area coverage data on mass-based N and P concentration and LMA in forest canopy foliage, in this case sampling a total of 2,045,379 ha distributed across 76 million ha of the Peruvian Andes–Amazon region. A geospatial modeling approach was then applied to the spectrometer data to derive relationships between LES traits and both climatic and geophysical factors throughout the study region (Fig. 1). We focused on this region

because it is an important part of the tropical forest biome containing a wide range of conditions (18). From hot lowland rainforests to treeline forests at almost 4,000 m above sea level, and from low to high fertility soils, this region provides a macrocosm in which to explore environmental controls on LES traits and address two questions. (i) Which climatic and geophysical factors control the geographic distribution of LES traits in humid tropical forest canopies? (ii) Do climatic and geophysical filters alter relationships between LES traits?

Results and Discussion

Regional Functional Diversity. Airborne imaging spectroscopy indicated previously unknown variation in forest canopy foliar N, P, and LMA throughout the Andes–Amazon region (Fig. 2). We

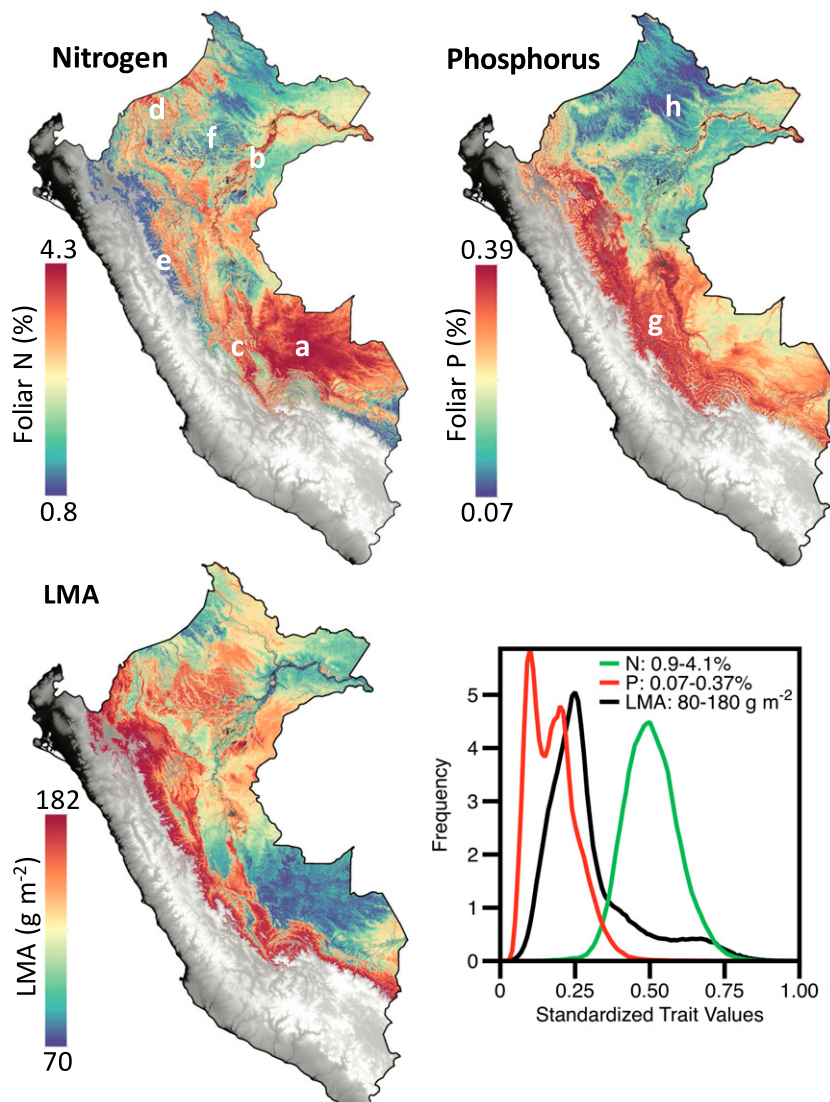


Fig. 2. Maps of forest canopy foliar N, P, and LMA throughout the Peruvian Andes and Amazon region. Inset graph shows the distributions of N, P, and LMA for the entire study region.

emphasize that our foliar N and P maps and resulting interpretations are presented on a dry mass basis. N and P ranged from 0.8–4.3% and 0.07–0.39%, respectively, at our mapping resolution of 1 ha. LMA varied from 64 to 182 g m⁻². In comparison, a database of globally distributed collections of individual leaves reports a range of 0.8–3.9% and 0.04–0.35% for N and P, respectively, and 20–220 g m⁻² for LMA, for 95% of their ranges (11). Given that our 1-ha resolution trait values each represent community-weighted averages taken over a hectare of forest canopy, and thus are integrative of hundreds of species and thousands of leaves per spectral measurement, our reported data ranges are large and globally relevant.

Geographic Trait Patterns. Within this highly variable LES environment, we observed geospatially complex trait patterns, with the underlying drivers of this variation expressed at multiple ecological scales (Fig. 2). To our knowledge, these are the first spatially explicit descriptions of canopy nutrients and LMA over a large portion of the terrestrial biosphere. Foliar N hotspots (>3.0% N) were found in forest canopies on: (i) substrates uplifted northeast of the geologic feature known as the Fitzcar-

rald Arch (Fig. 2, a); (ii) large floodplains along the Ucayali and Amazon rivers (Fig. 2, b); (iii) valleys in the eastern Andean foothills (Fig. 2, c); and (iv) relatively high-fertility substrates in the far northwestern Peruvian Amazon (Fig. 2, d). The N hotspot associated with the Fitzcarrald Arch is geographically aligned with geologic uplift and the occurrence of vast swaths of canopy bamboo (*Guadua* spp.) (19), which maintains high foliar N concentrations of 3.1–3.4% (20). Elevated foliar N in both Andean valley and lowland floodplain forest canopies is associated with high-fertility sediment deposition from montane sources (21). Northwestern high-N substrates have dual origin: exposed Pebas soils dating to the early Miocene (22), and more recent basaltic soils derived from volcanic flows starting in Ecuadorian Andes (23).

Foliar N coldspots (<2.0%) were found in montane forests, particularly on steep hillslopes (Fig. 2, e). Tropical montane forests are generally viewed as N-limited ecosystems, relative to their lowland tropical forest counterparts (24–26). Particularly low soil N is known to occur on steep portions of hilly or montane tropical terrain, a result of low N residence time in soils (27). Our results suggest that low soil N in both tropical mountains and on steep slopes is expressed in low canopy foliar N.

Low N was also common in lowland swamp forests in the Pastaza-Marañon foreland basin and elsewhere in particularly low-lying portions of the Amazon (Fig. 2, f). Low N in swamp canopies is linked to anoxic conditions, slow decomposition, and hyperdominance of *Mauritia flexuosa* (28), with known low foliar N (17).

Canopy foliar N was generally anticorrelated with mapped LMA, as is predicted by LES theory (Fig. 2). LMA increased with elevation, as observed in field-based altitudinal gradient studies (4, 29), along with decreasing foliar N. However, the strength of this relationship varied greatly and weakened under low-temperature conditions at higher elevations, discussed later in this report (see *Trait Interrelationships*, below). There were also strong and geographically extensive variations in LMA within the Amazonian lowlands, such as high LMA in palm swamps and on *terra firme*, as well as low LMA in bamboo-dominated forests (21).

Canopy foliar P displayed a spatial distribution much different from that of N and LMA (Fig. 2). Whereas N values were normally distributed throughout the Andes–Amazon region, P had a bimodal distribution. The higher mode at 0.25% P was primarily associated with the Andean foothill transition to the lowland Amazon (Fig. 2, g). Close inspection of this region revealed localized hotspots of P in Andean valley bottoms as well as within erosional incisions on uplifted surfaces in the Amazonian lowlands. These hotspots repeated in topographically explicit patterns associated with channel erosion. Whereas N was high in the eastern portion of the Fitzcarrald Arch (Fig. 2, a), P was elevated only within the western extreme relief of the Arch, particularly in intercrest (trough) depositional areas within this geologic formation. This pattern was also found in depositional areas within forests in the Andean foothills and montane region.

We discovered widespread suppression of foliar P in northern lowland forests of Peru (Fig. 2, h). This region is the source of the lower modal value of about 0.10% P in the regional distribution (Fig. 2, Inset graph). The lowest P values were found in areas underlain by Early Miocene substrate, and secondarily on younger Late Miocene substrate, in agreement with field work completed in that region (22). Relatively low P was mapped to the east of the Fitzcarrald Arch along the Peru–Brazil border, a region underlain by low-fertility substrates of Tertiary origin (30).

Drivers of Trait Variation. Geospatial modeling indicated that elevation and substrate were codominant determinants of the geographic distributions in N, P, and LMA measured with airborne imaging spectroscopy (Fig. 3). Because elevation and mean annual temperature are tightly correlated in the Andes–Amazon region (31), whereas precipitation and cloud cover are not (32), elevation and temperature are used synonymously when interpreting our results. Although substrate was relatively more important than elevation in determining N patterns, elevation was more important in explaining the geography of LMA. Following these two environmental filters, a small suite of additional climatic and topographic factors contributed to the LES trait patterns. Mean annual precipitation (MAP) and relative elevation (REM), which together serve as spatial predictors of soil moisture and local drainage conditions, were secondarily important in determining regional variation in N and LMA. In contrast, topographic slope and solar insolation were relatively important in explaining P patterns. All other factors played smaller roles in explaining the geography of each LES trait.

Because substrate type and elevation were the most important variables explaining all three LES traits (Fig. 3), we further assessed these particular factors. Normalized distributions of N, P, and LMA proved highly sensitive to the type of substrate underlying lowland Amazonian forests (Fig. 4, Fig. S5, and Tables S1 and S2). In the northern lowlands underlain by Miocene clays and white sands, canopy foliar P was deeply suppressed, leading to a relative high in canopy N in the map (Fig. 4, red). The exception was the Pastaza-Marañon foreland basin, where subsidence associated with about 120,000 km² of peatland (33)

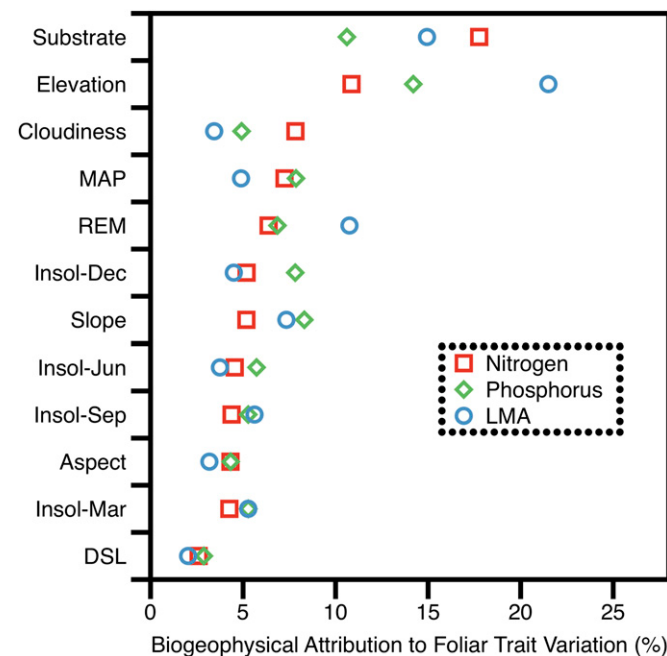


Fig. 3. Attribution of biogeophysical filters to forest canopy foliar N, P, and LMA throughout the Andes–Amazon region at 1-ha resolution. Substrate is derived from the geological map of Peru. Elevation, slope, aspect, and REM are derived from NASA SRTM data. Cloudiness, seasonal insolation (Insol-Dec, -Jun, -Sep, and -Mar) and dry season length are derived from NASA Tropical Rainfall Measuring Mission data.

(SPS in Fig. 4) results in forest canopies with exceedingly high LMA relative to N and P. In contrast to the relative partitioning of LES traits in northern Peruvian lowlands, the central and southern lowlands had relatively high N or P, depending upon physiographic position. The lowland Amazonian region of geologic uplift northeast of the Fitzcarrald Arch contained tree canopies with relatively high foliar N and P (FAS in Fig. 4, orange). The more central region of Andean deposition contains forest canopies with relatively high foliar P (HPS in Fig. 4, green).

Assessing LES trait responses to elevation, we found that N was high but variable at elevations less than about 700 m above sea level (Fig. 5A). Peak N values exceeding 2.7% at 1-ha resolution occurred in the 400- to 500-m elevation range. Foliar N declined to lowest values of about 2.1% above 2,000 m elevation. Foliar P followed a contrasting trend with elevation (Fig. 5B): very low lying areas (<100 m), where alluvial deposition is greatest, had locally high P values (0.135%), but then declined at slightly higher elevations of 100–400 m in the Amazon lowlands. This pattern is driven by differences between floodplain forests containing enriched alluvium from the Andes and upland *terra firme* forests on dystrophic clay soils (34). P concentrations then increased to a mean of ~0.15% at about 700-m elevation, and remained elevated to the Andean treeline. LMA responses to elevation inversely tracked N, even in the lowland *terra firme* regions (100–300 m above sea level), where LMA is subtly elevated compared with lower-lying floodplains (17). LMA asymptotically increased with elevation, but did not reach saturation.

Trait Interrelationships. Intercomparing the 1-ha resolution mapping results, we found major elevation-dependent differences in forest canopy foliar trait relationships (Fig. 6). N and LMA were inversely related in lowland and lower submontane forests (<1,100 m) (Fig. 6A). At these lower elevations, however, regression coefficients associating N and LMA varied from adjusted $R^2 = 0.25$ –0.58 (Fig. 7). Close inspection of the N-LMA regressions by topo-edaphic

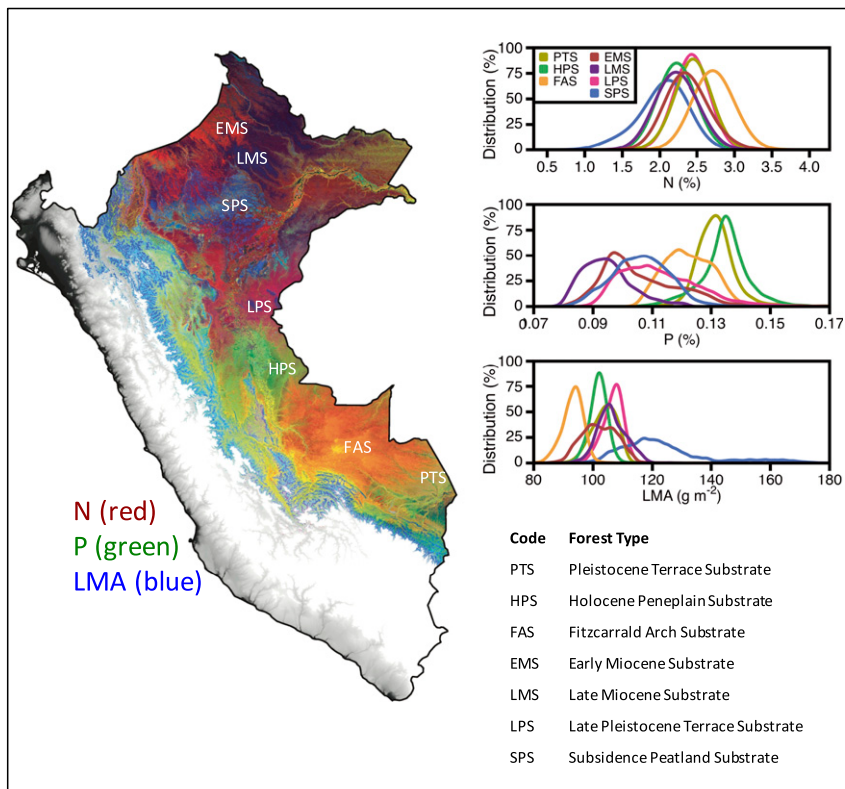


Fig. 4. Combined relative spatial variation in forest canopy foliar N, P, and LMA in the Andes–Amazon region at 1-ha resolution. Each trait is scaled from zero to unity, to allow for an assessment of relative dominance. The distributions of these traits for seven major lowland geological substrate types are shown to the right, color-coded to match the map. Additional detail on these lowland substrate types is provided in Table S1.

location revealed stronger N–LMA anticorrelations in alluvial and colluvial deposition zones (Fig. 7). These areas contain soils with much higher concentrations of rock-derived nutrients, including P and base cations (35), which subsequently support higher overall nutrient levels in forest canopy foliage (34). Nitrogen is generally held in higher concentrations in tropical forest canopies on soils with higher rock-derived nutrient availability, in part because of increased N fixation rates on higher-fertility soils (36, 37). Lowland forests situated on substrates with higher P availability presented a more linear inverse relationship between N and LMA.

Increases in elevation from the Andean foothills to treeline were met with an overall weakening of N–LMA anticorrelations in forest canopies (Figs. 6A and 7). However, a subregional increase in regression coefficient values, from adjusted $R^2 = 0.22$ at 1,500 m to 0.32 at 2,500-m elevation, was observed and may be a result of decreasing cloud inundation and thus solar radiation effects on the N–LMA relationship (38, 39). Above 2,500 m, however, N–LMA regression correlations declined sharply to 0.19 (Fig. 7). We also found that these elevation-dependent decreases in the N–LMA correlation resulted primarily from a truncation of the LMA range: whereas the foliar N range decreased by 25% relative to lowland forests, the LMA range collapsed by 55% (Fig. 6A). This finding agrees with field studies on elevation gradients suggesting that community-scale adaptations to decreasing temperature are more strongly expressed in foliar structure than in N concentration (40, 41). Notably, decreasing forest canopy LMA in the Andes is known to occur in conjunction with decreasing canopy compositional and functional diversity (21, 42).

In contrast to the N–LMA relationship, we found no evidence for a P–LMA or N–P correlation in Andean or Amazonian forest canopies (Fig. 6B and C). Instead, we detected a continuum of LES trait interactions that proved sensitive to elevation. One

strategy of high N+P and low LMA dominated lower submontane forest canopies of 400- to 1,000-m elevation. These canopies tended to be found on alluvium and colluvium sourced from Andean rock substrate. Another common strategy was low N, moderate P, and high LMA, which was found in upper submontane and montane forests (>1,000 m). Finally, the third strategy comprised of very low P, with highly variable N and LMA, was observed throughout the Amazonian lowlands. This strategy was again associated with low-fertility clay *terra firme* substrates.

The observed three-way interaction between N, P, and LMA indicates the existence of a continuum of adaptations to climatic (mainly temperature) and edaphic resource constraints. LMA, as a metric of carbon construction cost, responds to varying combinations of foliar N and P, each of which is differentially sensitive to climatic and edaphic conditions. Foliar N:P ratios have long been used to estimate relative changes in nutrient limitation to plant growth (43, 44), with extension to foliar construction cost and allocation studies (45, 46). We therefore computed the foliar N:P ratio of Peruvian forests, which revealed a regional gradient from high N:P in the Amazonian lowlands to low N:P in both Andean forests and depositional areas at the Andes–Amazon transition (Fig. 8). In the lowlands, N:P > 16 was observed in regions dominated by *terra firme*, including in extremely dystrophic northern forests and on elevated terrain associated with the uplift of the Fitzcarrald Arch. N:P ratios greater than 16 are generally representative of P limitation to productivity, relative to N availability, in humid tropical forests (47). In upper submontane and montane forests, N:P ratios < 16 suggest increasing N limitation relative to P, as recently detected in a field experiment in the Peruvian Andes (26). Low N:P was also found in particular portions of the Amazonian lowlands: extremely anoxic swamp environments are known areas of very low N availability relative to P (asterisks in Fig. 8) (17). Finally, it is

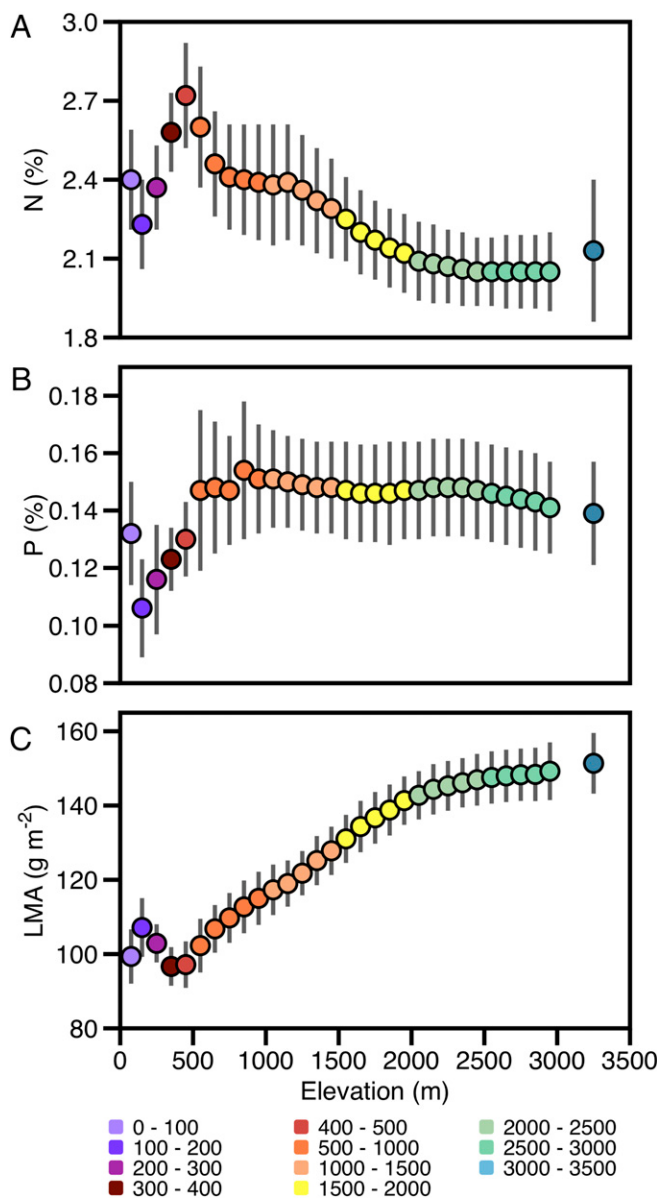


Fig. 5. (A–C) Changes in mean and SE (vertical bars) of N, P, and LMA with elevation for the entire Andes–Amazon study region. Elevation bands used to compile the results are listed at the bottom of the figure.

notable that our mapped N:P ratio results, to some degree, transcended issues of substrate type in the lowlands, suggesting overall P limitation in western lowland Amazonian forests. This finding, however, does not preclude the possibility of fine-scale effects of scarcity among other rock-derived nutrients (e.g., Ca, K, Mg) mediating forest function in lowland and montane ecosystems (48–50).

New Geography of LES Traits. The canopy foliar traits and interactions we have mapped and assessed shed new light on LES theory. Whereas the basic postulated inverse relationship between foliar N and LMA was mapped over significant portions of the Amazon region, a weakening of the relationship was observed at higher elevations as well as in multiple lowland forest settings. Substrate type and elevation (temperature) proved to be the strongest determinants of the N–LMA relationship, which was further mediated by other climatic and geophysical factors. This finding suggests that environmental filters generate more diverse ecosystem-scale physiological trade-offs than can be

captured in a universal leaf N–LMA interaction. In our case, the three-way interaction between N, P, and LMA observed throughout the study region was more indicative of multinutrient limitation of leaf construction cost and strategy, which has been proposed in some LES literature (1, 51). Although we did not remotely sense photosynthesis or its underpinning physiological components (but see ref. 52), variable N–P–LMA interactions likely reflect similarly variable nutrient–photosynthesis relationships (53, 54). We emphasize again that other nutrients, such as Ca, which cannot yet be measured well enough over large scales with imaging spectroscopy, are known correlates with leaf construction cost in tropical forests (21). A multinutrient LES geography will likely need to be extended to these essential elements in future mapping studies when they are more accurately detectable via remote sensing.

Beyond LES theory, functional traits are generally thought to be indicative of evolved plant adaptations to prevailing environmental conditions (55). In humid tropical forests, plant functional trait geography is also reflective of the assembly of species adapted to particular abiotic settings. For example, elevation and substrate sort both the composition (56) and functioning (21) of the tree canopy in Andean–Amazon forests, which in turn suggests that the hypothesis of neutral assembly (57) does not hold up at broad ecological scales in regions like the western Amazon. Why does this matter? Evolution and adaptation of functional traits mediating plant growth and survival under particular environmental conditions may generate limits to acclimation or migration in the face of rapid climate change. Others have similarly hypothesized the existence of such limits to functional plasticity (58), but the geography of potential trait adaptations have remained difficult to assess until now. Through our approach, key canopy foliar traits can now be quantitatively mapped, providing a functional biogeographic template against which to assess change, or the lack of change, over time.

To our knowledge, our study is the first to quantify the direction, strength, and geography of LES trait interactions at biospheric scales. Creating this functional biogeography provides an opportunity to improve our understanding of diverse controls on primary productivity, decomposition, and other fundamental

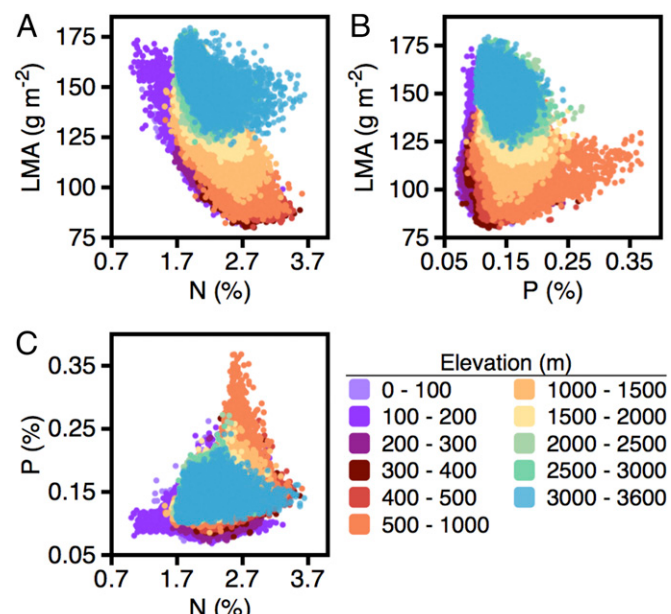


Fig. 6. (A–C) Relationships between forest canopy foliar N, P, and LMA in discrete elevation bands throughout the Andes–Amazon study region.

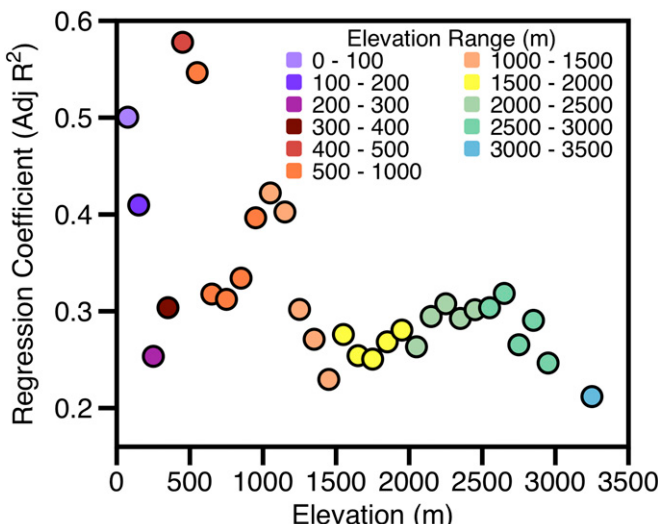


Fig. 7. Changes in the regression coefficient between forest canopy foliar N and LMA (from Fig. 6A) with increasing elevation.

biospheric processes. In tropical forest regions, for example, it is generally said that P limits productivity on highly weathered soils, such as those found in humid lowland settings (37, 59). In submontane to montane tropical settings, relative nutrient limitation may shift more to N or Ca (21, 26). Despite these basic prognostications, the relative strength and adaptation of the forest canopy to N, P, or cation supply remains poorly known at any ecological scale. The ability to map and assess N:P ratio and similar metrics provides a biogeophysically explicit basis upon which to assess previous or plan future field studies to test the role of nutrient limitation in mediating ecological processes. Similarly, these maps can serve as new input to the next generation of ecosystem, dynamic vegetation, and climate models, which are beginning to rely on LES traits and their interrelationships to simulate vegetation responses to environmental change (6, 60, 61). Future airborne, and perhaps space-based, studies of LES traits will open new doors to understanding and modeling the functional assembly of the biosphere and its responses to climate change.

Methods

Airborne Canopy Trait Sampling. We sampled the study region in 2012–2013 using the Carnegie Airborne Observatory (CAO) Airborne Taxonomic Mapping System (AToMS) (62). Prestratification of the region was carried out to ensure a spatially robust acquisition of airborne samples relative to a surface geology map (63), digital elevation model from the NASA Shuttle Radar Topography Mission (SRTM), and a forest ecosystems map of Peru (64) (Fig. 1 and Fig. S1). These stratification maps were gridded into 100×100 -km sectors, and the CAO was flown to randomly sample an average 3% of each classified stratum within each mapping sector (equating to about 30,000 ha per 100×100 -km sector). The airborne sampling totaled 2,045,379 ha.

CAO-AToMS instruments used for this study included a high-fidelity visible-to-shortwave infrared (VSWIR) imaging spectrometer and a dual laser, waveform LiDAR. We collected the data from an altitude of 2,000 m (± 250 m) above ground level, an average flight speed of 60 m s^{-1} , and a mapping swath of $\sim 1,200$ m. The VSWIR spectrometer measures spectral radiance in 427 channels spanning the 350- to 2,510-nm wavelength range in 5-nm increments (full-width at half-maximum). The spectrometer has a 34° field-of-view and an instantaneous field-of-view of 1 mrad. From 2,000 m above ground level, the spectral data were collected at 2.0-m ground sampling distance, or pixel size, throughout each study landscape. The LiDAR has a beam divergence of 0.5 mrad, and was operated at 200 kHz with 17° scan half-angle from nadir, providing swath coverage similar to the spectrometer. The LiDAR point density was four laser shots per m^{-2} . The total number of spatially unique spectral and LiDAR samples was 5.11 and 20.45 billion, respectively.

The LiDAR data were used to precisely geolocate the spectral data, and to provide a means to mask out canopy gaps and shadows, land use, water, and

exposed soil in the spectral data. To achieve this end, the laser ranges were combined with embedded high-resolution Global Positioning System-Inertial Measurement Unit data to determine the 3D locations of laser returns, producing a “cloud” of LiDAR data. The LiDAR data cloud consists of a very large number of georeferenced point elevation estimates, where elevation is determined relative to a reference ellipsoid. We used these points to interpolate a raster digital terrain model (DTM) for the ground surface of each landscape, which was achieved using a 10×10 -m kernel, with the lowest elevation estimate in each kernel assumed to be ground. Subsequent points were evaluated by fitting a horizontal plane to each of the ground seed points. If the closest unclassified point was $< 5.5^\circ$ and < 1.5 m higher in elevation, it was classified as ground. The digital surface model (DSM) was based on interpolations of all first-return points. Measurement of the vertical difference between the DTM and DSM yielded a digital canopy model of vegetation height above ground.

The method for mapping of canopy foliar chemical traits and LMA was developed and validated by Asner et al. (16). The method provides automated processing of imaging spectrometer datasets over large geographic areas, while minimizing localized effects of varying sun-sensor-canopy geometry, inter- and intracrown shading, forest gaps, land use, and terrain-related artifacts. A data-fusion approach, facilitated by the collection of boresight-aligned spectral and LiDAR measurements, underpins the method, as reported by Asner et al. (65). The approach removes pixels unsuitable for sunlit canopy spectroscopic measurement, including noncanopy surfaces, shaded canopy pixels, and pixels with low foliar content. To achieve this, the LiDAR was used to measure the height of the vegetation within each spectral pixel, and to model intercanopy shade between pixels. Only vegetation taller than 2 m in height was analyzed for canopy foliar traits. To ensure that spectral pixels have sufficient foliar content, a minimum Normalized Difference Vegetation Index threshold of 0.8 was also applied. Spectral pixels that met these criteria were considered suitable for canopy trait analysis, and those spectra were averaged at a mapping resolution of 1 ha.

Before conversion from spectra to canopy trait estimates, the spectral data were radiometrically corrected from raw digital number values to radiance ($\text{W sr}^{-1}/\text{m}^{-2}$) using a flat-field correction, radiometric calibration coefficients, and spectral calibration data that had been collected in the laboratory before each flight campaign. The spectral data were precisely colocated to the LiDAR data via a camera model that determines the 3D location and field-of-view of each sensor element, and combines it with standardized timing information. A smoothed best estimate of trajectory, the LiDAR DTM, and the camera model were then used to produce an image geometry model and observational data containing information on solar and viewing geometry for each image pixel. These inputs were used to atmospherically correct the radiance imagery using the ACORN-5 model (Imspec LLC). To improve aerosol corrections in ACORN-5, we iteratively ran the model with different visibilities until the reflectance at 420 nm (which is relatively constant for vegetated pixels) was 1%. Reflectance imagery was corrected for cross-track brightness gradients using a bidirectional reflectance distribution function modeling approach described by Colgan et al. (66). The imaging spectrometer data were then orthorectified to the LiDAR digital canopy model.

Following the preparation of the filtered 1-ha resolution spectra, we convolved the data to 10-nm bandwidth and applied a brightness-normalization adjustment (67). This reduced the contribution of varying leaf area index to chemometric determinations of foliar traits from remotely sensed data (68). The resulting spectra were trimmed at the far ends (400 nm, 2,500 nm) of the measured wavelength range, as well as in regions dominated by atmospheric water vapor (1350–1480, 1780–2032 nm) that blocks a spectral reflectance signal. We used partial least-squares regression (69) to convert the 1-ha resolution spectral data to foliar N, P, and LMA estimates using the method validated by Asner et al. (16). The spectral dependence of N, P, and LMA is shown in Fig. S2. The partial least-squares regression approach is beneficial because it uses the continuous spectrum as a single measurement rather than in a band-by-band type of analysis (70, 71). Across 79 1-ha field plots in Peru, Asner et al. (16, 17) showed that LMA could be retrieved with an uncertainty (root mean squared error or RMSE) of 11.8 g m^{-2} across a LMA range of 76 – 180 mg g^{-1} . The average uncertainty of leaf N and P mapping was 0.30% and 0.02%, respectively (N range = 1.28–4.33%; P range = 0.06–0.36% by mass).

Modeling. We used the Random Forest Machine Learning algorithm (RFML) (72) to model the spatial relationship between 1-ha resolution LES traits derived from airborne sampling and a suite of spatially extensive geophysical datasets (Fig. 1). RFML fits multiple decision trees to input data (e.g., spatially coincident environmental datasets) using a random subset of the input variables for each tree constructed for a given response variable (e.g., airborne LES samples). The modal value of the calculated decision trees is used to create an “ensemble” tree that is used for prediction. RFML is nonparametric, relatively insensitive to

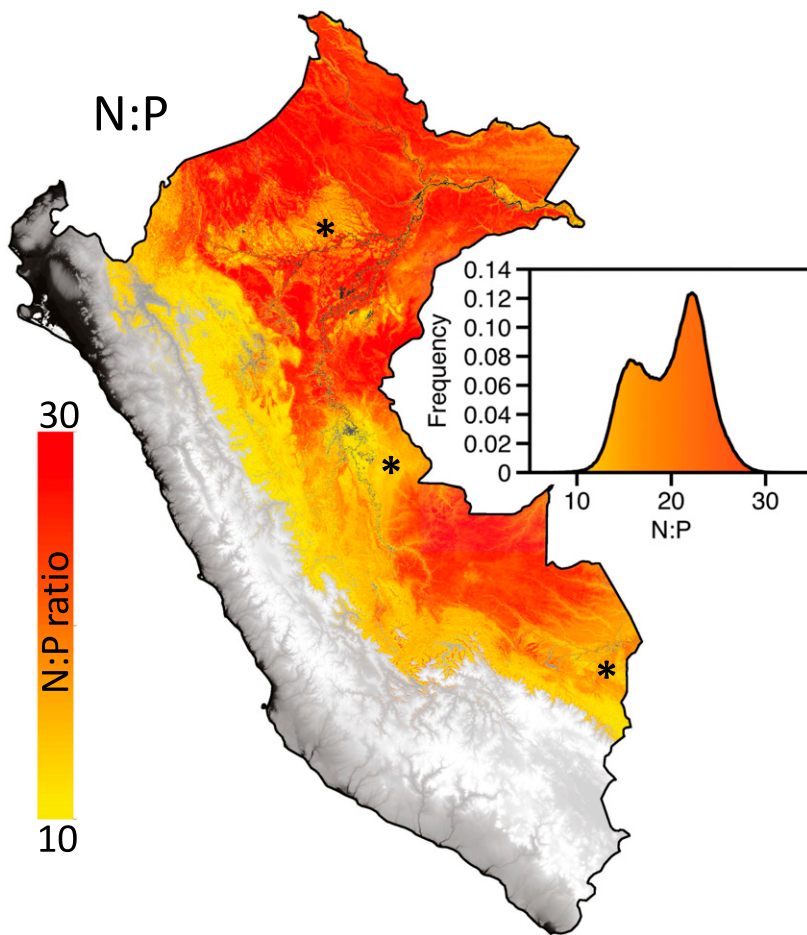


Fig. 8. Ecological variation in forest canopy foliar N:P ratio at 1-ha resolution throughout the Andes–Amazon study region. The inset graph provides a frequency distribution for all values in the map.

data skew, and robust to a high number of variable inputs (73). This approach has been used extensively to scale remotely sensed samples of forest structure and biomass to regional and biome levels (e.g., refs. 74 and 75).

The environmental variables used in the RFML models for each canopy trait were taken from coaligned predictor spatial datasets (Fig. S3). We included a geology map of Peru (63). We also used topographic variables derived from NASA SRTM data at 90-m resolution: ground elevation, slope, and aspect. A REM was also developed by calculating the height of the ground above the nearest water body (75), thus providing a spatial proxy for vegetation-related water resources. We also included MAP data derived from 12 y of NASA Tropical Rainfall Measurement Mission observations, as well as long-term (2000–2010) cloudiness data derived from the NASA Moderate Resolution Imaging Spectroradiometer (MODIS). Cloudiness is based on the number of times a MODIS pixel was identified as being affected by clouds in the quality assurance flags of the 8-d reflectance product (76). We developed multiple potential incoming solar insolation models using SRTM elevation data in the SAGA GIS Potential Insolation module (77). These insolation layers (units of kilowatt h/m²) were created by modeling total insolation (direct and diffuse) for the days of the equinoxes and solstices (March 21, June 21, September 21, and December 21). We used Landsat imagery with the CLASlite forest mapping system to define forest cover

throughout the region (78). Environmental data maps were resampled to 1-ha resolution, coaligned, and combined into a stack of predictor variables covering Andean and Amazonian forests of Peru.

Model Verification. Seventy-nine 1-ha field plots (see ref. 16) were used to check that the modeled canopy traits were in agreement with those estimated directly from airborne imaging spectroscopy (Fig. S4). Results indicate that N, P, and LMA area were modeled with relatively high precision and accuracy, as estimated via R^2 values and RMSE, relative to spectrometer-based estimates (N: $R^2 = 0.64$, RMSE = 0.12%; P: $R^2 = 0.67$, RMSE = 0.01%; LMA: $R^2 = 0.92$, RMSE = 3.5 g m⁻²).

ACKNOWLEDGMENTS. We thank R. Tupayachi, F. Sinca, N. Jaramillo, L. Carranza-Jimenez, P. Martinez, and others in the Carnegie field team for supporting underpinning aspects of this work; and P. Taylor and the two reviewers for constructive comments on the manuscript. We gratefully acknowledge our long-term collaboration with the Peruvian Ministry of Environment. This study was funded by the John D. and Catherine T. MacArthur Foundation. The Carnegie Airborne Observatory is made possible by the Avatar Alliance Foundation, John D. and Catherine T. MacArthur Foundation, Grantham Foundation for the Protection of the Environment, Mary Anne Nyburg Baker and G. Leonard Baker Jr., and William R. Hearst III.

1. Wright IJ, et al. (2004) The worldwide leaf economics spectrum. *Nature* 428(6985): 821–827.
2. Finegan B, et al. (2015) Does functional trait diversity predict above-ground biomass and productivity of tropical forests? Testing three alternative hypotheses. *J Ecol* 103(1):191–201.
3. Santiago LS, Wright SJ (2007) Leaf functional traits of tropical forest plants in relation to growth form. *Funct Ecol* 21(1):19–27.
4. Poorter H, Niinemets U, Poorter L, Wright IJ, Villar R (2009) Causes and consequences of variation in leaf mass per area (LMA): A meta-analysis. *New Phytol* 182(3):565–588.
5. Vitousek PM (1984) Litterfall, nutrient cycling, and nutrient limitation in tropical forests. *Ecology* 65(1):285–298.
6. Sakschewski B, et al. (2015) Leaf and stem economics spectra drive functional diversity in a dynamic global vegetation model. *Glob Change Biol* 21(7):2711–2725.

7. Moles AT, et al. (2014) Which is a better predictor of plant traits: temperature or precipitation? *J Veg Sci* 25(5):1167–1180.
8. Wright IJ, et al. (2005) Assessing the generality of global leaf trait relationships. *New Phytol* 166(2):485–496.
9. Schimel D, et al. (2015) Observing terrestrial ecosystems and the carbon cycle from space. *Glob Change Biol* 21(5):1762–1776.
10. Reich PB, Oleksyn J (2004) Global patterns of plant leaf N and P in relation to temperature and latitude. *Proc Natl Acad Sci USA* 101(30):11001–11006.
11. Kattge J, et al. (2011) TRY—A global database of plant traits. *Glob Change Biol* 17(9): 2905–2935.
12. Townsend AR, Asner GP, Cleveland CC (2008) The biogeochemical heterogeneity of tropical forests. *Trends Ecol Evol* 23(8):424–431.
13. Kokaly RF, Asner GP, Ollinger SV, Martin ME, Wessman CA (2009) Characterizing canopy biochemistry from imaging spectroscopy and its application to ecosystem studies. *Remote Sens Environ* 113:S78–S91.
14. Ustin SL, et al. (2009) Retrieval of foliar information about plant pigment systems from high resolution spectroscopy. *Remote Sens Environ* 113:S67–S77.
15. Goetz AFH, Vane G, Solomon JE, Rock BN (1985) Imaging spectrometry for Earth remote sensing. *Science* 228(4704):1147–1153.
16. Asner GP, Martin RE, Anderson CB, Knapp DE (2015) Quantifying forest canopy traits: Imaging spectroscopy versus field survey. *Remote Sens Environ* 158:15–27.
17. Asner GP, et al. (2015) Landscape biogeochemistry reflected in shifting distributions of chemical traits in the Amazon forest canopy. *Nat Geosci* 8(7):567–573.
18. Hoorn C, et al. (2010) Amazonia through time: Andean uplift, climate change, landscape evolution, and biodiversity. *Science* 330(6006):927–931.
19. de Carvalho AL, et al. (2013) Bamboo-dominated forests of the southwest Amazon: Detection, spatial extent, life cycle length and flowering waves. *PLoS One* 8(1): e54852.
20. Asner GP, Martin RE (2011) Canopy phylogenetic, chemical and spectral assembly in a lowland Amazonian forest. *New Phytol* 189(4):999–1012.
21. Asner GP, et al. (2014) Amazonian functional diversity from forest canopy chemical assembly. *Proc Natl Acad Sci USA* 111(15):5604–5609.
22. Higgins MA, et al. (2011) Geological control of floristic composition in Amazonian forests. *J Biogeogr* 38(11):2136–2149.
23. Räsänen ME, Salo JS, Jungnert H, Pittman LR (1990) Evolution of the Western Amazon lowland relief: Impact of Andean foreland dynamics. *Terra Nova* 2(4):320–332.
24. Tanner EVJ, Vitousek PM, Cuevas E (1998) Experimental investigation of nutrient limitation of forest growth on wet tropical mountains. *Ecology* 79(1):10–23.
25. Adamek M, Corre MD, Hölscher D (2009) Early effect of elevated nitrogen input on above-ground net primary production of a lower montane rain forest, Panama. *J Trop Ecol* 25(6):637–647.
26. Fisher JB, et al. (2013) Nutrient limitation in rainforests and cloud forests along a 3,000-m elevation gradient in the Peruvian Andes. *Oecologia* 172(3):889–902.
27. Weintraub SR, et al. (2014) Topographic controls on soil nitrogen availability in a lowland tropical forest. *Ecology* 96(6):1561–1574.
28. Goodman RC, et al. (2013) Amazon palm biomass and allometry. *For Ecol Manage* 310:994–1004.
29. Körner C, Farquhar GD, Wong SC (1991) Carbon isotope discrimination by plants follows latitudinal and altitudinal trends. *Oecologia* 88(1):30–40.
30. Asner GP, et al. (2010) High-resolution forest carbon stocks and emissions in the Amazon. *Proc Natl Acad Sci USA* 107(38):16738–16742.
31. Metcalfe DB, et al. (2014) Herbivory makes major contributions to ecosystem carbon and nutrient cycling in tropical forests. *Ecol Lett* 17(3):324–332.
32. Halladay K, Malhi Y, New M (2012) Cloud frequency climatology at the Andes/Amazon transition: 1. Seasonal and diurnal cycles. *J Geophys Res, D, Atmospheres* 117(D23).
33. Lähteenoja O, et al. (2012) The large Amazonian peatland carbon sink in the sub-siding Pastaza-Marañón foreland basin, Peru. *Glob Change Biol* 18(1):164–178.
34. Fyllas N, et al. (2009) Basin-wide variations in foliar properties of Amazonian forest: Phylogeny, soils and climate. *Biogeosciences* 6(11):2677–2708.
35. Quesada C, et al. (2009) Regional and large-scale patterns in Amazon forest structure and function are mediated by variations in soil physical and chemical properties. *Biogeosciences* 6(2):3993–4057.
36. Houlton BZ, Wang Y-P, Vitousek PM, Field CB (2008) A unifying framework for di-nitrogen fixation in the terrestrial biosphere. *Nature* 454(7202):327–330.
37. Vitousek PM, Porder S, Houlton BZ, Chadwick OA (2010) Terrestrial phosphorus limitation: Mechanisms, implications, and nitrogen-phosphorus interactions. *Ecol Appl* 20(1):5–15.
38. Aranda I, Pardo F, Gil L, Pardos J (2004) Anatomical basis of the change in leaf mass per area and nitrogen investment with relative irradiance within the canopy of eight temperate tree species. *Acta Oecol* 25(3):187–195.
39. Ellsworth DS, Reich PB (1993) Canopy structure and vertical patterns of photosynthesis and related leaf traits in a deciduous forest. *Oecologia* 96(2):169–178.
40. Cordell S, Goldstein G, Meinzer FC, Handley LL (1999) Allocation of nitrogen and carbon in leaves of *Metrosideros polymorpha* regulates carboxylation capacity and delta 13C along an altitudinal gradient. *Funct Ecol* 13(6):811–818.
41. Körner C, Bannister P, Mark AF (1986) Altitudinal variation in stomatal conductance, nitrogen content and leaf anatomy in different plant life forms in New Zealand. *Oecologia* 69(4):577–588.
42. Gentry AH (1988) Changes in plant community diversity and floristic composition on environmental and geographical gradients. *Ann Mo Bot Gard* 75(1):1–34.
43. Vitousek PM, Denslow JS (1986) Nitrogen and phosphorus availability in treefall gaps of a lowland tropical rainforest. *J Ecol* 74:1167–1178.
44. McGroddy ME, Daufresne T, Hedin LO (2004) Scaling of C:N:P stoichiometry in forests worldwide: Implications of terrestrial Redfield-type ratios. *Ecology* 85(9):2390–2401.
45. Reich PB, Schoettle AW (1988) Role of phosphorus and nitrogen in photosynthetic and whole plant carbon gain and nutrient use efficiency in eastern white pine. *Oecologia* 77(1):25–33.
46. Niinemets U, Kull K (2003) Leaf structure vs. nutrient relationships vary with soil conditions in temperate shrubs and trees. *Acta Oecol* 24(4):209–219.
47. Townsend AR, Cleveland CC, Asner GP, Bustamante MMC (2007) Controls over foliar N:P ratios in tropical rain forests. *Ecology* 88(1):107–118.
48. Chadwick KD, Asner GP (2016) Tropical soil nutrient distributions determined by biotic and hillslope processes. *Biogeochemistry* 127(2):1–17.
49. Wright SJ, et al. (2011) Potassium, phosphorus, or nitrogen limit root allocation, tree growth, or litter production in a lowland tropical forest. *Ecology* 92(8):1616–1625.
50. Townsend AR, Cleveland CC, Houlton BZ, Alden CB, White JW (2011) Multi-element regulation of the tropical forest carbon cycle. *Front Ecol Environ* 9(1):9–17.
51. Reich PB, Oleksyn J, Wright IJ (2009) Leaf phosphorus influences the photosynthesis–nitrogen relation: A cross-biome analysis of 314 species. *Oecologia* 160(2):207–212.
52. Doughty C, Asner G, Martin R (2011) Predicting tropical plant physiology from leaf and canopy spectroscopy. *Oecologia* 165(2):289–299.
53. Evans JR (1989) Photosynthesis and nitrogen relationships in leaves of C₃ plants. *Oecologia* 78(1):9–19.
54. Field C, Mooney HA (1986) The photosynthesis–nitrogen relationship in wild plants. *On the Economy of Plant Form and Function*, ed Givnish TJ (Cambridge Univ Press, Cambridge, UK), pp 25–55.
55. Violette C, Reich PB, Pacala SW, Enquist BJ, Kattge J (2014) The emergence and promise of functional biogeography. *Proc Natl Acad Sci USA* 111(38):13690–13696.
56. Baldeck C, Tupayachi R, Sinca F, Jaramillo N, Asner G (2015) Environmental drivers of tree community turnover in western Amazonian forests. *Ecography*.
57. Hubbell SP (2001) *The Unified Neutral Theory of Biodiversity and Biogeography* (Princeton Univ Press, Princeton).
58. Read QD, Moorhead LC, Swenson NG, Bailey JK, Sanders NJ (2014) Convergent effects of elevation on functional leaf traits within and among species. *Funct Ecol* 28(1): 37–45.
59. Cleveland CC, et al. (2011) Relationships among net primary productivity, nutrients and climate in tropical rain forest: A pan-tropical analysis. *Ecol Lett* 14(9):939–947.
60. Schimel DS, Asner GP, Moorcroft PR (2013) Observing changing ecological diversity in the Anthropocene. *Front Ecol Environ* 11(3):129–137.
61. Moorcroft PR (2006) How close are we to a predictive science of the biosphere? *Trends Ecol Evol* 21(7):400–407.
62. Asner GP, et al. (2012) Carnegie Airborne Observatory-2: Increasing science data dimensionality via high-fidelity multi-sensor fusion. *Remote Sens Environ* 124(0):454–465.
63. INGEMMET (2000) *Mapa Geológico del Perú* (Instituto Geológico Minero y Metalúrgico, Lima).
64. Asner GP, et al. (2014) Targeted carbon conservation at national scales with high-resolution monitoring. *Proc Natl Acad Sci USA* 111(47):E5016–E5022.
65. Asner GP, et al. (2007) Carnegie Airborne Observatory: In-flight fusion of hyper-spectral imaging and waveform light detection and ranging for three-dimensional studies of ecosystems. *J Appl Remote Sens* 1:013536.
66. Colgan MS, Baldeck CA, Féret J-B, Asner GP (2012) Mapping savanna tree species at ecosystem scales using support vector machine classification and BRDF correction on airborne hyperspectral and LiDAR data. *Remote Sens* 4(11):3462–3480.
67. Feilhauer H, Asner GP, Martin RE, Schmidlein S (2010) Brightness-normalized partial least squares regression for hyperspectral data. *J Quant Spectrosc Radiat Transf* 111: 1947–1957.
68. Asner GP, et al. (2011) Spectroscopy of canopy chemicals in humid tropical forests. *Remote Sens Environ* 115(12):3587–3598.
69. Haaland DM, Thomas EV (1988) Partial least-squares methods for spectral Analyses. 1. Relation to other quantitative calibration methods and the extraction of qualitative information. *Anal Chem* 60(11):1193–1202.
70. Boulesteix A-L, Strimmer K (2007) Partial least squares: A versatile tool for the analysis of high-dimensional genomic data. *Brief Bioinform* 8(1):32–44.
71. Martens H (2001) Reliable and relevant modelling of real world data: A personal account of the development of PLS Regression. *Chemom Intell Lab Syst* 58(2):85–95.
72. Breiman L (2001) Random forests. *Mach Learn* 45(1):5–32.
73. Evans JS, Murphy MA, Holden ZA, Cushman SA (2011) Modeling species distribution and change using random forest. *Predictive Species and Habitat Modeling in Landscape Ecology: Concepts and Applications*, eds Drew CA, Wiersma YF, Huettmann F (Springer Science, New York), pp 139–159.
74. Baccini A, et al. (2012) Estimated carbon dioxide emissions from tropical deforestation improved by carbon-density maps. *Nat Clim Change* 2(3):182–185.
75. Mascaro J, et al. (2014) A tale of two “forests”: Random forest machine learning AIDS tropical forest carbon mapping. *PLoS One* 9(1):e85993.
76. NASA Land Processes Distributed Active Archive CenterDAAC (2011) MOD09A1. (USGS Earth Resources Observation and Science, Sioux Falls, SD).
77. Cimberly V (2010) *User Guide for SAGA (version 2.0.5)*. Available at www.saga-gis.org. Accessed June 22, 2016.
78. Asner GP, Knapp DE, Balaji A, Paez-Acosta G (2009) Automated mapping of tropical deforestation and forest degradation: CLASlite. *J Appl Remote Sens* 3:033543.

Supporting Information

Asner et al. 10.1101/1604863113

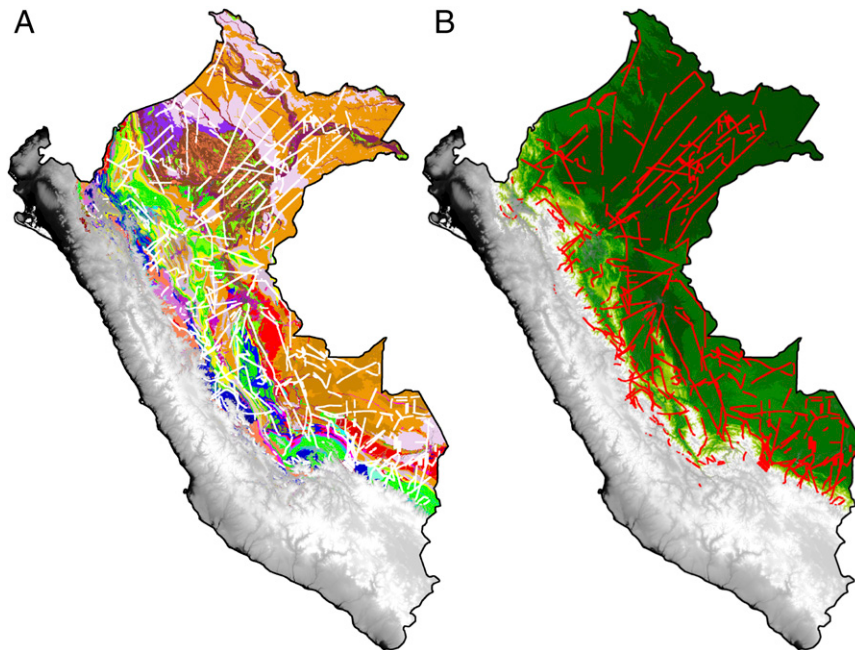


Fig. S1. Spatial distribution of CAO flightlines, each 1.2 km in mapping swath, throughout the Andes–Amazon study region. The background maps are (A) geologic substrate and (B) elevation.

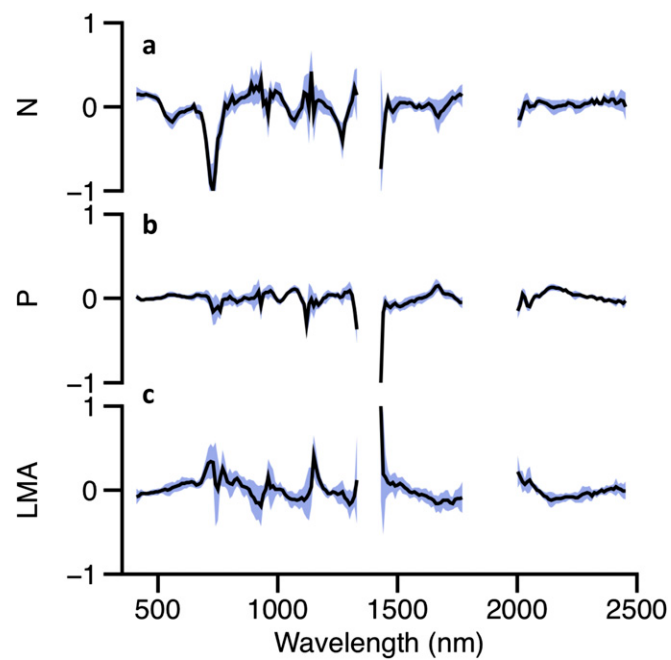


Fig. S2. Chemometric spectral weightings associating mass-based (A) nitrogen and (B) phosphorus concentrations, and (C) LMA, with wavelength-dependent reflectance from 400 to 2,500 nm using the Carnegie Airborne Observatory (CAO) Visible-to-Shortwave Infrared (VSWIR) imaging spectrometer. Data from ref. 16.

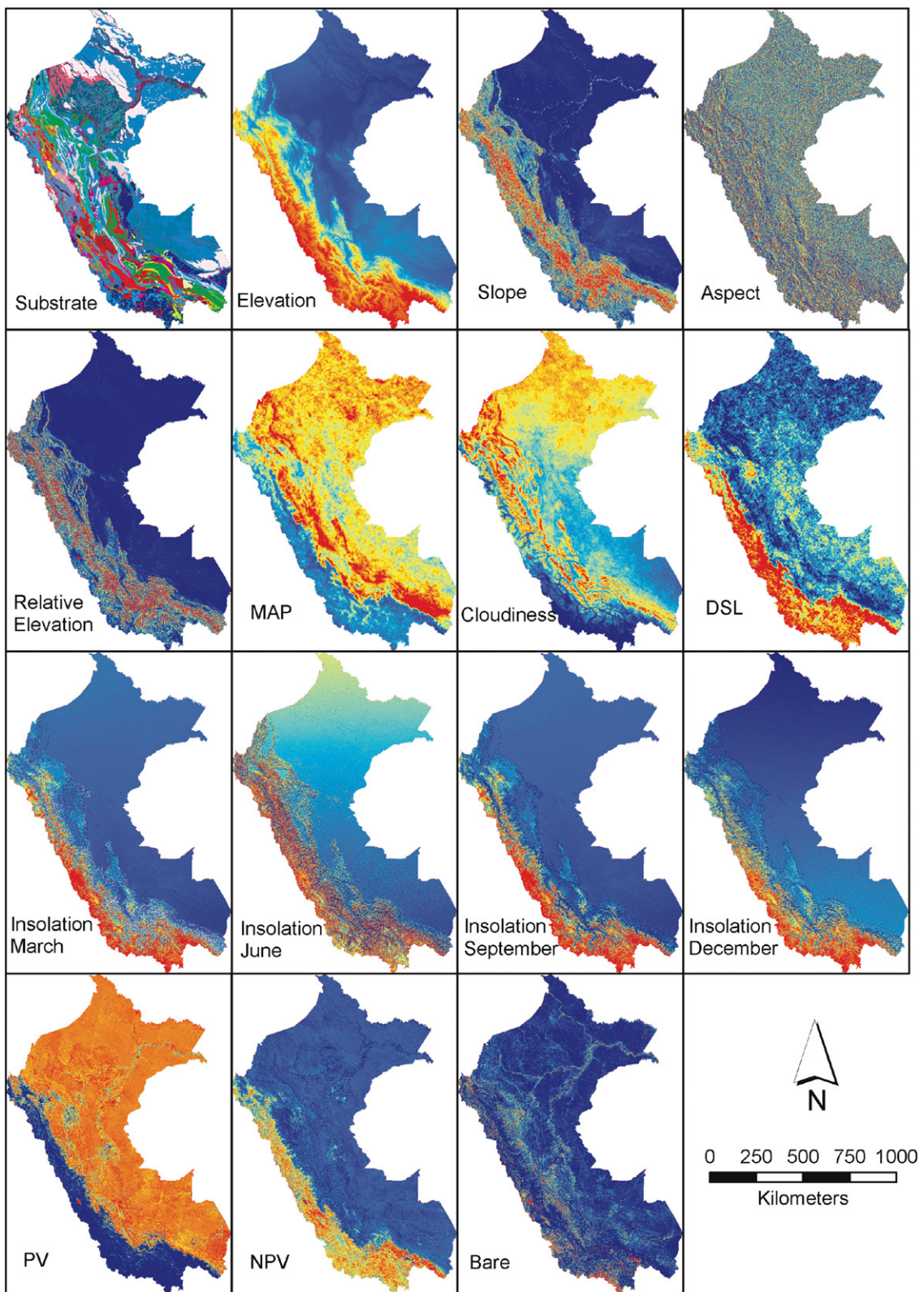


Fig. S3. Input data layers used for biogeophysical modeling and upscaling of the airborne imaging spectrometer data. Bare, bare substrate (soils, rocks, and so forth); DSL, day season length; MAP, mean annual precipitation; NPV, nonphotosynthetic vegetation; PV, photosynthetic vegetation.

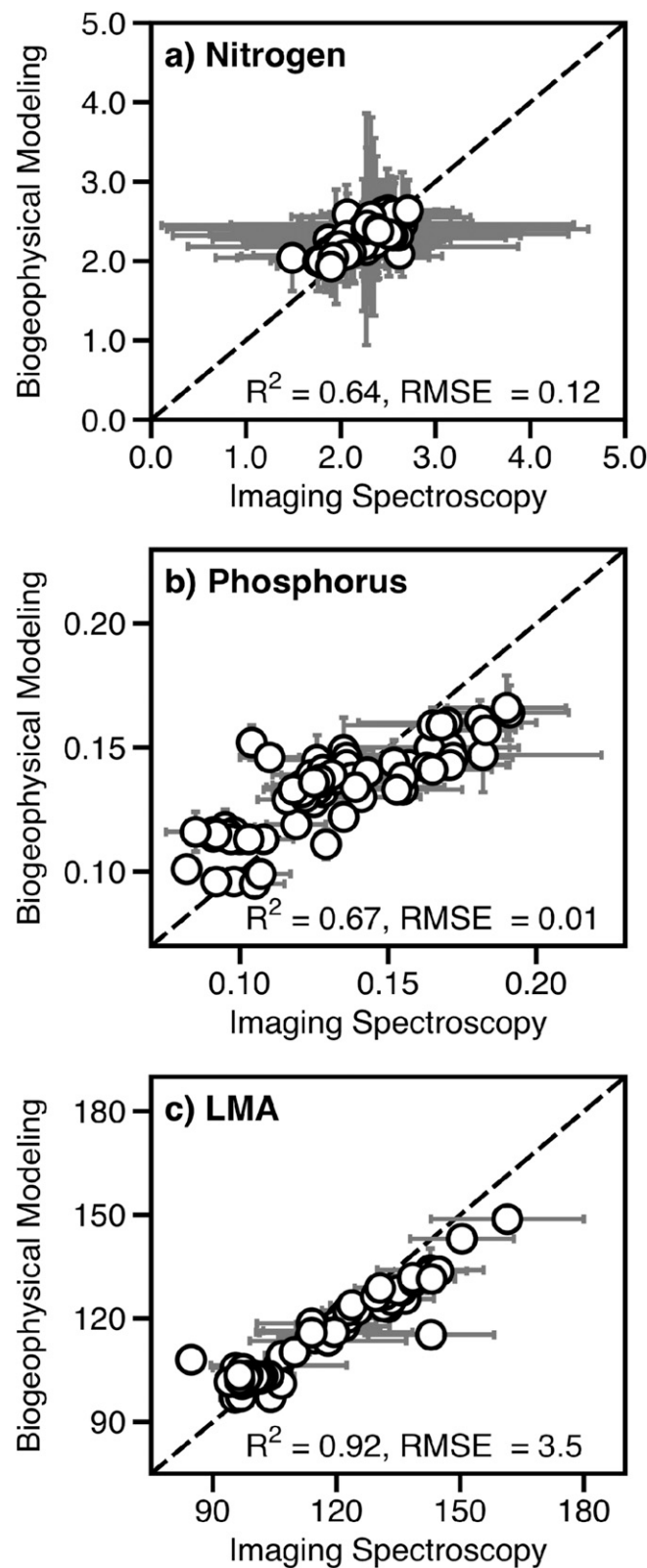


Fig. S4. Evaluation of remotely sensed versus modeled mass-based (A) nitrogen and (B) phosphorus concentrations, and (C) LMA, for 79 1-ha field verification plots spread throughout the Peruvian Andes and Amazon region (see ref. 16 for plot locations).

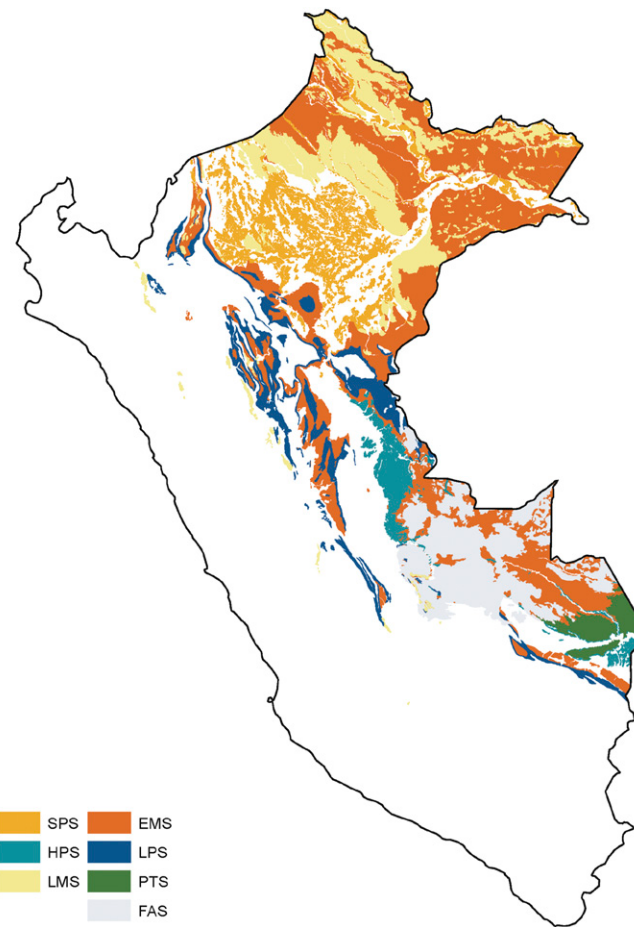


Fig. S5. Regional distribution of the seven primary geologic substrates underlying the forests of the lowland Peruvian Amazon. These substrates were used in the analyses presented in Fig. 4 and are described in Tables S1 and S2.

Table S1. Leaf economics spectrum traits in canopies in western lowland Amazonian forests

Code	Mapped forest type	N	P	LMA
EMS	Early Miocene substrate	2.37 ± 0.20	0.106 ± 0.014 ^B	102.1 ± 5.8 ^C
LMS	Late Miocene substrate	2.23 ± 0.18 ^A	0.095 ± 0.008	106.3 ± 4.8
SPS	Subsidence peatland substrate	2.04 ± 0.27	0.106 ± 0.010 ^B	123.7 ± 15.6
LPS	Late Pleistocene terrace substrate	2.43 ± 0.08	0.112 ± 0.013	106.8 ± 3.5
HPS	Holocene peneplain substrate	2.22 ± 0.14 ^A	0.135 ± 0.008	101.9 ± 2.9 ^C
FAS	Fitzcarrald Arch substrate	2.72 ± 0.17	0.122 ± 0.008	93.1 ± 3.5
PTS	Pleistocene terrace substrate	2.44 ± 0.12	0.132 ± 0.009	103.8 ± 4.2

Each trait was statistically different by forest type (ANOVA with Tukey's HSD multiple comparisons; $P < 0.05$) unless noted with a matching superscript letter.

Table S2. Foliar trait moments for mapped forest canopies throughout the lowland portion of western Amazonia

N, P, LMA	EMS	FAS	HPS	LMS	LPS	PTS	SPS
N (%)							
Mean	2.37	2.72	2.22 ^A	2.23 ^A	2.43	2.44	2.04
SD	0.20	0.17	0.14	0.18	0.08	0.12	0.27
CV	8.52	6.43	6.07	8.10	3.42	4.79	13.20
Skew	0.80	0.17	0.09	0.26	-0.69	-0.74	-0.88
Kurtosis	0.76	-0.31	0.02	-0.61	2.26	1.71	0.56
Minimum	1.85	2.17	1.85	1.75	1.98	1.88	1.21
Maximum	3.27	3.38	2.78	2.87	2.77	2.90	2.74
Range	1.42	1.20	0.93	1.12	0.79	1.02	1.53
P (%)							
Mean	0.106 ^B	0.122	0.135	0.095	0.112	0.132	0.106 ^B
SD	0.014	0.008	0.008	0.008	0.013	0.009	0.010
CV	13.05	6.69	6.29	8.84	11.41	6.55	9.17
Skew	1.12	0.29	0.19	0.74	0.69	3.98	0.16
Kurtosis	2.06	-0.09	2.65	0.42	0.27	37.93	0.19
Minimum	0.076	0.102	0.098	0.074	0.080	0.106	0.077
Maximum	0.192	0.167	0.187	0.122	0.168	0.310	0.152
Range	0.116	0.066	0.089	0.048	0.088	0.204	0.075
LMA (g m ⁻²)							
Mean	102.1 ^C	93.1	101.9 ^C	106.3	106.8	103.8	123.7
SD	5.8	3.5	2.9	4.8	3.5	4.2	15.6
CV	5.72	3.75	2.89	4.52	3.25	4.00	12.57
Skew	-0.01	-0.35	-0.18	0.24	-0.22	-0.36	1.17
Kurtosis	83.69	78.95	86.67	90.23	94.62	86.85	89.28
Minimum	83.7	79.0	86.7	90.2	94.6	86.8	89.3
Maximum	126.0	106.3	116.1	126.8	125.6	119.1	178.6
Range	42.3	27.4	29.4	36.5	30.9	32.3	89.3

Distributions of forest types are shown in Fig. 4. Results sharing a superscript are not statistically different (*t* tests; *P* < 0.05). See Table S1 for definition of each forest type. CV is coefficient of variation.